Scattering versus forbidden decay in dark matter freeze-in

Shao-Ping Li*

Institute of High Energy Physics, Chinese Academy of Sciences, Beijing 100049, China

(Received 5 December 2022; accepted 5 July 2023; published 12 July 2023)

It is generically believed that the two-body scattering is suppressed by higher-order weak couplings with respect to the two-body decay. We show that this does not always hold when a heavy particle is produced by a forbidden decay in a thermal plasma, where the scattering shares the same order of couplings with the decay. We find that there is a simple and close relation between the forbidden decay and the same-order scattering. To illustrate this point, we consider the freeze-in production of heavy dark matter via a light scalar mediator. We point out that when the Boltzmann (quantum) statistics is used, the forbidden decay can contribute to the dark matter relic density at 5%–24% (10%–39%) with a weak thermal coupling, while the contribution from the scattering channel can be several orders of magnitude larger than from the forbidden decay if the thermal coupling is much smaller. Such a relative effect between the scattering and the forbidden decay could also exist in other plasma-induced processes, such as the purely thermal generation of the right-handed neutrino dark matter, or of the lepton asymmetry in leptogenesis.

DOI: 10.1103/PhysRevD.108.015014

I. INTRODUCTION

In many theories beyond the Standard Model (SM) of particle physics, a heavy species can be usually produced by a light particle in a thermal plasma. This kind of production, which is kinematically forbidden in vacuum but opened at finite temperatures due to plasma effects, has been studied in a wide range of phenomena, such as the dark matter (DM) production [1–8], the production of neutrinos from plasmon decay in stellar cooling [9–13], and the thermally induced baryon asymmetry in the early Universe [14–25].

In the scenarios of forbidden decay, the two-body scattering mediated by the light particle can also be significant and even dominate the production. A known example is the neutrino chirality-flipping process $\nu_L \to \nu_R$ in the relativistic QED plasma, where the contribution from the t-channel scattering $e + \nu_L \to e + \nu_R$ was found to be much larger than from the plasmon decay $\gamma^* \to \bar{\nu}_L + \nu_R$, since the latter is suppressed by a higher-order electromagnetic coupling $\alpha_{\rm EM}$ [26–29]. A similar effect is also found recently in the electron chirality-flipping process [30,31]. For a nonthermal DM produced via the freeze-in paradigm [32–36], it has been shown that the forbidden two-body decay can be the dominant mechanism (see, e.g., Refs. [1,5,37]) and in some cases, be the unique channel to account for the DM relic density [6,8].

The two-body scattering is generically expected to be suppressed by higher-order weak couplings, which results in the two-body decay being the dominant channel for most situations. However, when the decay channel is a purely plasma-induced effect, the two-body scattering associated with the very forbidden decay can carry the same order of coupling constants. To see this, we show an example in Fig. 1 with the scalar forbidden decay to fermions via the Yukawa interaction $y_\chi \bar{\chi}\chi\phi$. For a vacuum mass condition $m_\phi < 2m_\chi$, the scalar decay $\phi \to \bar{\chi} + \chi$ is kinematically forbidden in vacuum but opened at temperatures above some critical point $T_c = 2m_\chi/\kappa$ as the light scalar ϕ acquires temperature-dependent thermal mass $m_\phi(T) \equiv \kappa T$ from, e.g., the Yukawa interaction $y_\psi \bar{\psi}\psi\phi$. Here, κ characterizes the correction factor from the thermal plasma, which is encoded in the red blob of Fig. 1. Since a nonzero κ is induced by the resummed self-energy in the red blob, it points out that the scattering $\bar{\psi} + \psi \to \bar{\chi} + \chi$ mediated by the light scalar also exists when the forbidden decay is opened. This can be seen by cutting the red blob in the forbidden decay diagram such that the loop particles go on shell while the scalar becomes off shell. With such a cut, the scattering channel is said to be hinted from the forbidden decay diagram.

As will be derived in this paper, both the scattering and forbidden decay rates can carry the same order of coupling prefactor $\propto y_\chi^2 y_\psi^2$. It differs from the usual vacuum situations where the scattering carries higher-order weak couplings and also from the chirality-flipping processes where the scattering channel carries a lower-order

*spli@ihep.ac.cn

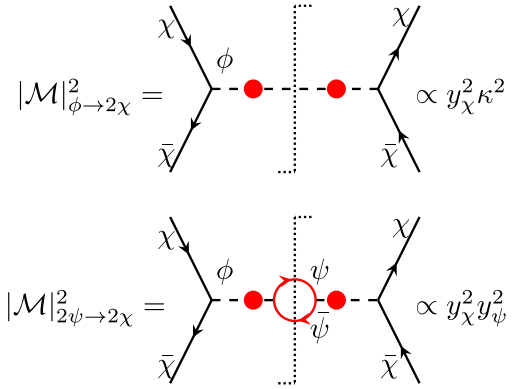

FIG. 1. The scattering channel $\bar{\psi}+\psi\to\bar{\chi}+\chi$ associated with the forbidden decay $\phi\to\bar{\chi}+\chi$ at the same order of coupling prefactor $y_\psi^2 y_\chi^2$, where $\kappa\sim y_\psi$ is generically expected when the thermal correction (red blob) to ϕ dominantly arises from a self-energy topology similar to the red one.

electromagnetic coupling as mentioned above. Without the suppression (enhancement) of higher (lower)-order weak couplings in the scattering channel, it could be nontrivial to see the relative effect of the plasma-induced decay and the scattering. In particular, whenever nonthermal DM production with a light thermal mediator is concerned, it would be tempting to know the portion from mediator forbidden decay when the conventional scattering via a light mediator is considered [38]. On the other hand, whenever the forbidden decay from a light mediator can account for the DM relic density [1,5,6,8,37], it would be necessary to check if the scattering effect is indeed suppressed.

In this paper, we consider a close relation between the renormalizable forbidden decay and the associated scattering channel in freeze-in DM production via a light mediator. To illustrate the key formulation for comparing the scattering with the forbidden decay, we consider in the remainder of this paper, a light scalar mediator shown in Fig. 1, where the nonthermal fermion χ is a DM candidate having a direct freeze-in channel from the scalar forbidden decay $\phi\to\bar{\chi}+\chi$. The close relation to be shown can be simply characterized by the dominant coupling that helps the mediator to equilibrate with the thermal plasma. Moreover, the simple relation allows us to estimate the relative contribution of the forbidden decay and scattering in producing the observed DM relic density.

As will be shown below, the scattering effect can dramatically modify the forbidden decay scenarios of DM production at finite temperatures. In particular, the ratio of the relic density from the scattering to that from the forbidden decay has a simple scaling $\sim 1/y_\psi$ in the weak-coupling limit $y_\psi < 1$. It implies that the contribution from the forbidden decay can only become significant for a large thermal coupling, and if not, the scattering contribution will be orders of magnitude larger than from the pure decay channel.

We expect that the close relation can also exist in a wide range of scenarios, such as the millicharged DM [39,40] generated from the plasmon decay [5], the right-handed neutrino DM [41,42] from a thermal scalar decay [3], or even the nonthermal DM production from a hidden thermal plasma [43,44]. We further expect that it could modify the pattern of leptogenesis when the out-of-equilibrium generation of lepton asymmetries results from forbidden decay in the early Universe [14,22–25]. The investigation presented here complements the widely studied plasma-induced effects at finite temperatures where the two-body decay and the scattering generically carry different powers of coupling prefactors.

II. RELATIVE RATES OF FORBIDDEN DECAY AND SCATTERING

Let us first point out that the scattering effect at high temperatures could be already comparable to the forbidden decay rate. The heavy DM χ can be produced by a light thermal scalar ϕ which establishes thermal equilibrium with a light fermion ψ in the plasma. The relevant interaction is characterized by

$$\mathcal{L} = y_\chi\bar{\chi}\chi\phi + y_\psi\bar{\psi}\psi\phi. \tag{1}$$

We consider the situation where thermal particles ϕ,ψ are much lighter than the nonthermal χ at zero temperature so that the nonrelativistic $\bar{\psi}\psi$ annihilation to χ is kinematically forbidden in vacuum. In practice, the subsequent calculations are approximately obtained by taking $m_{\phi,\psi}(T=0)=0$. It should be mentioned, however, when the vacuum masses of the thermal particles are compatible with m_χ, significant corrections could arise. For simplicity, we further assume that the dominant thermal correction to ϕ can be well encapsulated by the $\bar{\psi}\psi\phi$ interaction. Including other comparable corrections opens additional scattering channels associated with the forbidden decay. While we are not devoted to specific scenarios, it it noteworthy that realistic models can already be constructed from (1). For example, the scalar is a SM singlet and couples to a light Majorana neutrino ψ which can readily equilibrate with the SM plasma via neutrino oscillation [45,46].

A special exception that the scattering channel hinted from the forbidden decay diagram may be suppressed is the $\lambda\phi^4$ theory, which generates $\kappa\propto\sqrt{\lambda}$ at leading order [47]. The $\lambda\phi^4$ interaction can also induce a ϕ^3 vertex $\propto\lambda v_\phi$ when ϕ develops a nonzero vacuum expectation value v_ϕ. Then, besides the additional dependence on v_ϕ, the collision rate from the scattering $\phi+\phi\to\bar{\chi}+\chi$ has a higher-order λ prefactor than from the forbidden decay $\phi\to\bar{\chi}+\chi$ and would be suppressed by small λ. Nevertheless, when λ is small, the scattering comparable with the forbidden decay can still be opened from, e.g., a gauge scalar-vector-vector $B_\mu B^\mu\phi$ or a trilinear-scalar $\phi\Phi^2$ interaction. Therefore, the

same-order scattering associated with the forbidden decay can be a generic result when the dominant thermal correction arises from a self-energy diagram similar to the red bubble in Fig. 1.

From (1), the squared amplitude in the forbidden decay $\phi \to \bar{\chi} + \chi$ reads

$$|\mathcal{M}|^2_{\phi\to 2\chi} = 2y_\chi^2(\kappa^2 T^2 - 4m_\chi^2). \tag{2}$$

The Boltzmann equation for the evolution of χ number density is given by

$$\dot{n}_\chi + 3Hn_\chi = 2\gamma_{\phi\to 2\chi}, \tag{3}$$

where the Hubble parameter reads $H \approx 1.66\sqrt{g_\rho}T^2/M_{\rm Pl}$, with $M_{\rm Pl} = 1.22 \times 10^{19}$ GeV the Planck mass and g_ρ the effective degrees of freedom for the energy density. The factor of 2 results from the χ-pair production. The collision rate from Eq. (2) reads

$$\gamma_{\phi\to 2\chi} = \frac{\kappa^3 y_\chi^2 K_1(\kappa)}{16\pi^3}\left(1 - \frac{4m_\chi^2}{\kappa^2 T^2}\right)^{3/2} T^4, \tag{4}$$

where $K_1(\kappa)$ is the modified Bessel function with $K_1(\kappa) \approx 1/\kappa$. Note that in obtaining the collision rate in the Boltzmann equation, we apply the Boltzmann distribution $f = e^{-E/T}$ for the thermal particles, and the Pauli-blocking effect from the nonthermal DM χ is neglected. To make a comparison between the Boltzmann approximation and the full quantum statistics for the thermal particles, we will perform the analysis of the full quantum statistics whenever relevant in the subsequent discussions. For the moment, it suffices to take the Boltzmann distribution as an approximation to analyze the relative effect of the scattering and forbidden decay channels.

The scattering production for the nonthermal DM χ occurs through the s channel $\bar{\psi} + \psi \to \bar{\chi} + \chi$. With the usual treatment in vacuum, the cross section without the spin average of ψ is simply given by

$$\sigma_{2\psi\to 2\chi} = \frac{y_\chi^2 y_\psi^2}{4\pi s}\left(1 - \frac{4m_\chi^2}{s}\right)^{3/2}. \tag{5}$$

The resulting collision rate with the Boltzmann statistics then reads [48]

$$\gamma_{2\psi\to 2\chi} \approx \frac{T}{32\pi^4}\int_{4m_\chi^2}^\infty ds \sigma_{2\psi\to 2\chi} s^{3/2} K_1(\sqrt{s}/T). \tag{6}$$

It can be seen that, the scattering rate in this vacuum treatment can already be comparable to the forbidden decay rate if κ is at $\mathcal{O}(y_\psi)$. Explicitly, using $\kappa = y_\psi/\sqrt{6}$ to be derived below, we have the approximate relation,

$$\frac{\gamma_{2\psi\to 2\chi}}{\gamma_{\phi\to 2\chi}} \approx 0.3, \tag{7}$$

in the high-temperature limit $m_\chi/T \ll 1$. Note that, however, if the full quantum statistics is used, i.e., Fermi-Dirac distribution for the thermal fermion ψ and Bose-Einstein distribution for the thermal scalar ϕ, the ratio in Eq. (7) becomes 0.13. This suppression arises from the Pauli-blocking effects for ψ and Bose enhancement for ϕ.

Thus far, the cross section is only computed in the limit of $s \gg m_\phi^2(T)$, where the effect near the pole $s = m_\phi^2(T)$ is not taken into account properly. Since the cross section may be enhanced near the pole and both $\gamma_{\phi\to 2\chi}$ and $\gamma_{2\psi\to 2\chi}$ have the same prefactor dependence, the effect from such an s-channel enhancement could further increase the ratio given by Eq. (7). The resonant enhancement appears when the momentum transfer is at $\mathcal{O}(\kappa T)$. This soft-scattering transfer can come either from the soft $\bar{\psi}\psi$ pair with momenta at $\mathcal{O}(\kappa T)$, or from the collinear $\bar{\psi}\psi$ pair with hard momenta at $\mathcal{O}(T)$ but with a small angle at $\mathcal{O}(\kappa)$ between the $\bar{\psi}\psi$ momenta [49,50]. Under the perturbative hard-thermal-loop (HTL) technique [51–53] (see also, e.g., Refs. [47,54]), the thermal correction to ψ for hard $\bar{\psi}\psi$ pair is of higher order, while for soft $\bar{\psi}\psi$ pair, both the thermal correction to ψ and the resummed $\bar{\psi}\psi\phi$ vertex should be included to obtain a consistent result at leading order. Here, we consider the hard $\bar{\psi}\psi$ pair since a thermal relativistic particle has an averaged momentum at $\mathcal{O}(T)$.

Following the effective treatment in Ref. [49], we compute the cross section by including the leading-order thermal correction in the internal ϕ propagator and treating the external hard $\bar{\psi}\psi$ pair effectively massless. The cross section reads

$$\sigma_{2\psi\to 2\chi} = \frac{y_\chi^2 y_\psi^2}{4\pi\sqrt{s}}\frac{(s - 4m_\chi^2)^{3/2}}{[s - {\rm Re}\Pi_R^\phi]^2 + [{\rm Im}\Pi_R^\phi]^2}, \tag{8}$$

where Π_R^ϕ is the resummed retarded self-energy amplitude of ϕ. In the real-time formalism of thermal field theory [55,56], the real part of Π_R^ϕ is given by

$${\rm Re}\Pi_R^\phi = \frac{y_\psi^2}{\pi^3}\int d^4q f_\psi(\omega)\frac{k.q}{(k+q)^2}\delta(q^2), \tag{9}$$

where $f_\psi(\omega) = (e^{\omega/T} + 1)^{-1}$ is the Fermi-Dirac distribution function for ψ with $\omega \equiv |q_0|$ and k is the four-momentum of ϕ with $s = k^2$. In the HTL approximation, $k^2/|\vec{q}|^2 \sim \mathcal{O}(y_\psi^2)$ is of higher order. We neglect these high-order terms in the integral and obtain ${\rm Re}\Pi_R^\phi \approx y_\psi^2 T^2/6$. The dispersion relation of the thermal scalar ϕ is determined by the pole $k^2 - {\rm Re}\Pi_R^\phi = 0$, leading to $\kappa = y_\psi/\sqrt{6}$. On the other hand, the imaginary self-energy amplitude is given by

$$\mathrm{Im}\Pi_R^\phi = -\frac{y_\psi^2 k^2}{4\pi^2}\int d^4q[1-2f_\psi(\omega)]\delta_{k+q}\delta_q, \quad (10)$$

where the two Dirac δ functions $\delta_{k+q} \equiv \delta[(k+q)^2]$ and $\delta_q \equiv \delta(q^2)$ dictate that the loop particles go on shell.

Since the scattering has an s-channel resonance, the collision rate in the Boltzmann equation should be calculated without double counting [49]. There are several methods to remove the double counting [14,50,57–63]. Here, we follow Refs. [57,59,62] with a real-intermediate-state subtraction by splitting the Breit-Wigner form of the scalar propagator as

$$\begin{aligned} iG_\phi(p^2) &= \frac{i}{p^2 - m_\phi^2 + im_\phi\Gamma_\phi} \\ &= \frac{i(p^2-m_\phi^2)}{(p^2-m_\phi^2)^2 + m_\phi^2\Gamma_\phi^2} + \frac{m_\phi\Gamma_\phi}{(p^2-m_\phi^2)^2 + m_\phi^2\Gamma_\phi^2} \\ &\equiv iG_{\phi,\mathrm{off}}(p^2) + G_{\phi,\mathrm{on}}(p^2), \end{aligned} \quad (11)$$

where Γ_ϕ is the decay width of the thermal scalar. In practice, we use the thermal scalar mass, $m_\phi^2 = \mathrm{Re}\Pi_R^\phi$ and take $\Gamma_\phi = \mathrm{Im}\Pi_R^\phi(k^2 = m_\phi^2)/m_\phi$ to estimate the damping rate of the thermal scalar from the simplified Lagrangian (1). For off shell scattering, the scalar propagator is given by the off shell term $G_{\phi,\mathrm{off}}$. The off shell part from Eq. (8) is given by

$$\sigma_{2\psi\to 2\chi,\mathrm{off}} = \frac{y_\chi^2 y_\psi^2 \beta}{4\pi}\frac{s(s-m_\phi^2)^2}{[(s-m_\phi^2)^2 + m_\phi^2\Gamma_\phi^2]^2}, \quad (12)$$

with $\beta \equiv (1-4m_\chi^2/s)^{3/2}$, which is then substituted into Eq. (6) to obtain the collision rate in the Boltzmann approximation.

The comparison between the forbidden decay and the scattering is shown in Fig. 2. In the Boltzmann approximation, the ratio given in Eq. (7) at $T \gg T_c$ is kept for $y_\psi = 10^{-4}$–10^{-2} but enhanced to be $\gamma_{2\psi\to 2\chi,\mathrm{off}} \approx 0.81\gamma_{\phi\to 2\chi}$ for $y_\psi = 0.1$. Therefore, the relation in Eq. (7) can be lifted up by a factor of $\mathcal{O}(1)$ for a large thermal coupling y_ψ. With a large y_ψ, the thermal correction included in the propagator can partially compensate for the suppression of additional phase-space factors in the two-body scattering. When the full quantum statistics is used for the initial thermal particles, we found that $\gamma_{2\psi\to 2\chi,\mathrm{off}} \approx 0.13\gamma_{\phi\to 2\chi}$ for $y_\psi = 10^{-4}$–10^{-1}, which is the same as in the vacuum case as discussed below Eq. (7). It implies that the enhancement of the ratio $\gamma_{2\psi\to 2\chi,\mathrm{off}}/\gamma_{\phi\to 2\chi}$ due to large thermal corrections of the mediator propagator becomes less significant when the Pauli-blocking effects of the two thermal fermions and the Bose enhancement of the thermal scalar are accounted for in the collision rates.

When T evolves down to the threshold point $T_c = 2m_\chi/\kappa$ (the vertical dotted lines), the kinematic space for the forbidden decay tends to close, thereby exhibiting a sudden drop in the left panel of Fig. 2. Nevertheless, the scattering continues until T drops below m_χ, after which the scattering rate will carry a Boltzmann suppression factor $e^{-m_\chi/T}$, as shown by the drop of the collision curves.

Besides a potential $\mathcal{O}(1)$ enhancement near the resonance region, there is a more important effect after the decay channel closes. As seen in the left panel of Fig. 2, there is a period of χ production from the pure scattering channel while the duration of the forbidden decay depends on the thermal coupling y_ψ. For smaller y_ψ, the decay duration is shorter and hence, less χ production. This is explained by the fact that smaller y_ψ dictates a higher threshold temperature T_c, consequently leading to a shorter duration of the forbidden decay in the early Universe. This observation implies that the contribution from the

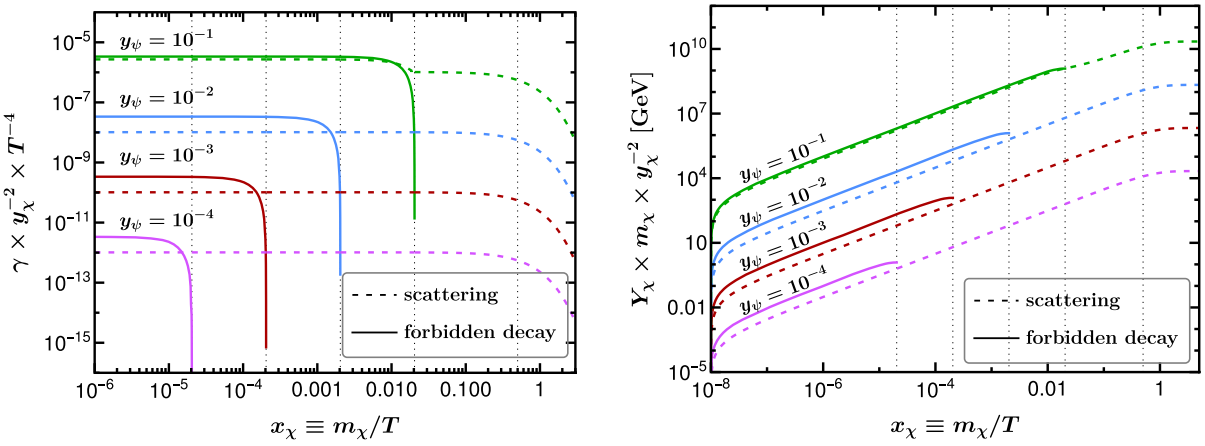

FIG. 2. Left: comparison of collision rates between the forbidden decay and the off shell scattering. The collision rates are normalized to the squared DM coupling y_χ^2 and the quartic temperature T^4. Right: comparison of DM yields Y_χ by factoring out the dependence on the DM mass m_χ and the DM coupling y_χ.

scattering can be much larger than from the forbidden decay if the pure scattering lasts sufficiently long in the expansion history of the Universe. We show in the right panel of Fig. 2 a complementary plot for the DM yield $Y_\chi \equiv n_\chi/s_{\rm SM}$ as a function of $x_\chi \equiv m_\chi/T$. It can be seen that the generation of Y_χ ends at the critical temperature (the vertical dotted lines) in the forbidden decay channel but continues below T_c in the scattering channel. It points out clearly that the final abundance from the forbidden decay channel can become comparable to the scattering channel when the thermal coupling y_ψ becomes large.

III. RELATIVE DM RELIC DENSITY

To see the relative contribution of the scattering and the forbidden decay to the DM relic density, we solve the Boltzmann equation of the DM number density yield from

$$Y_\chi \approx \int_{T_c}^{\infty} \frac{2\gamma_{\phi\to 2\chi}}{s_{\rm SM}HT}dT + \int_0^{\infty} \frac{2\gamma_{2\psi\to 2\chi,\rm off}}{s_{\rm SM}HT}dT, \quad (13)$$

where $s_{\rm SM} = g_s 2\pi^2 T^3/45$ is the SM entropy density with g_s the effective degrees of freedom, and $\gamma_{2\psi\to 2\chi,\rm off}$ is the off shell scattering rate. We have used the symbol $\approx$ above to highlight that the yield is approximately obtained in the limit of $m_{\phi,\psi}(T=0)=0$. The forbidden decay is closed at $T_c = 2m_\chi/\kappa$, and the scattering essentially ends around $T \simeq m_\chi$ but using $T=0$ as the lower limit in Eq. (13) does not cause significant difference. In the following, we will not distinguish the small difference between g_s and g_ρ, and simply set $g_s = g_\rho = 106.75$ which becomes a good approximation if the freeze-in temperature is well above the GeV scale [64].

To compare the relic densities produced from the forbidden decay and the scattering, we integrate the temperature analytically for $\gamma_{\phi\to 2\chi}$ and numerically for $\gamma_{2\psi\to 2\chi,\rm off}$, where the analytic relic density from the decay channel can be written as

$$\Omega_{\phi\to 2\chi}h^2 \approx 0.34\left(\frac{y_\psi}{0.1}\right)^3\left(\frac{y_\chi}{10^{-9}}\right)^2 \quad (14)$$

in the limit of a generically weak coupling $y_\psi \lesssim 1$ and the Boltzmann approximation.

Note that $\Omega_{\phi\to 2\chi} \propto y_\psi^3$ while $\gamma_{\phi\to 2\chi} \propto y_\psi^2$. The additional power dependence on the thermal coupling y_ψ comes from the fact that the freeze-in DM production is IR dominated, and both the decay $\phi \to \bar\chi + \chi$ and the annihilation $\bar\psi + \psi \to \bar\chi + \chi$ are kinematically forbidden at zero temperature, making the yield Y_χ depend on the inverse threshold temperature and the heavy DM mass scale. It can then be found that both $\Omega_{\phi\to 2\chi}$ and $\Omega_{2\phi\to 2\chi,\rm off}$ are basically independent of the DM mass. However, for the vacuum mass condition $m_\psi > m_\chi$, the annihilation $2\psi \to 2\chi$ is opened at zero temperature and the yield Y_χ would not have the simple $1/m_\chi$ dependence. This is the case for the sub-MeV or lighter DM production from the nonrelativistic electron-positron annihilation [5,37].

Independent of the DM mass, the ratio of $\Omega_{2\psi\to 2\chi,\rm off}$ to $\Omega_{\phi\to 2\chi}$ can then be simply estimated by the thermal coupling y_ψ, which is shown in the left panel of Fig. 3. Approximately, we find that the ratio in the Boltzmann statistics can be fitted as

$$\frac{\Omega_{2\psi\to 2\chi,\rm off}}{\Omega_{\phi\to 2\chi}} \approx 0.8y_\psi + 1.8y_\psi^{-1} + 0.5, \quad (15)$$

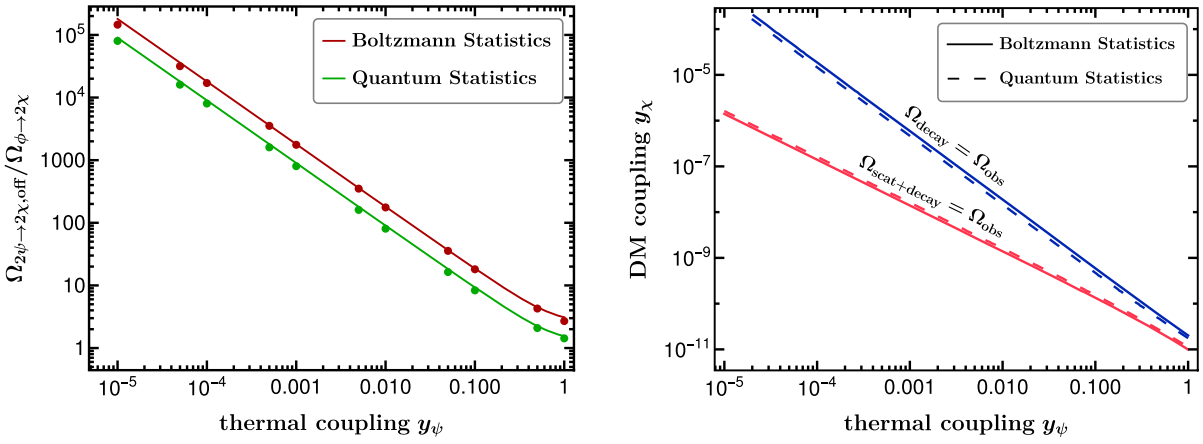

FIG. 3. Left: the relic density ratio of off shell scattering to forbidden decay. The selected points are obtained from full numerical results, while the solid lines are obtained from the fitted formula (15). Right: the correlation between the DM coupling y_χ and the thermal coupling y_ψ for the observed DM relic density obtained from the forbidden decay only and the sum of the forbidden decay and scattering channels, respectively. The results from the Boltzmann approximation and the full quantum statistics are shown as a comparison.

while the ratio in the full quantum statistics is approximately a factor of 2 smaller than in the Boltzmann statistics. For smaller thermal coupling y_ψ, the ratio basically scales as $1/y_\psi$. Taking $y_\psi = 10^{-3}$ for example, we can see that the DM relic density produced through the off shell scattering channel is a factor of 1800 larger than that through the forbidden decay; however, the ratio decreases below $\mathcal{O}(10)$ for an electroweak gauge coupling. When $y_\psi = 1$, the ratio in Eq. (15) gives $\Omega_{2\psi\to 2\chi,\mathrm{off}}/\Omega_{\phi\to 2\chi} \approx 3.1$. It indicates that the contribution to the DM relic density from the forbidden decay becomes significant when the thermal coupling is large. Typically, we expect a portion of 5%–24% (10%–39%) from the forbidden decay in the weak-coupling regime $0.1 \lesssim y_\psi \lesssim 1$ when the Boltzmann (quantum) statistics is used.

We can also see from the right panel of Fig. 3 the correlation between the nonthermal DM coupling y_χ and the thermal coupling y_ψ when the observed DM relic density $\Omega_{\mathrm{obs}}h^2 = 0.12$ [65] is accounted for by the sum of the forbidden decay and scattering channels. Besides, we also show the correlation when the DM relic density is only generated by the forbidden decay. As seen from the right panel of Fig. 3, when compared to the purely forbidden decay channel, the strong scattering contribution with a small thermal coupling opens up the parameter space of the DM coupling towards smaller values. We can also observe that the Boltzmann approximation does not lead to large discrepancies from the full quantum statistics.

IV. DISCUSSION

While we consider a simple scalar mediator here, the similar pattern between the scattering and the forbidden decay can also be expected in other light mediators [50]. For instance, a fermion DM coupling to the SM via a vector mediator (the photon) has been considered in Refs. [5,37]. It was demonstrated that the plasmon decay is the dominant channel for sub-MeV DM production. This can in fact be explained by Fig. 2. The effective photon thermal mass can be estimated by a correction factor $\kappa \sim \sqrt{\alpha_{\mathrm{EW}}} \sim \mathcal{O}(0.1)$ in the thermal plasma. For a sub-MeV DM, the threshold temperature can reach $T_c \sim 10^{-3}$ GeV and the sudden drop of the decay curve in Fig. 2 can be postponed until $m_\chi/T \simeq \mathcal{O}(0.1)$. When the temperature is above the electron mass m_e, the contributions from the plasmon decay and the electron-positron pair production are comparable. However, the pair production becomes Boltzmann suppressed when $T_c < T < m_e$, and the scattering curve in Fig. 2 would exhibit the drop prior to that in the decay curve. In this case, the scattering contribution is suppressed in the history of the production and the plasmon decay becomes the dominant channel. For much heavier DM, however, the production from the nonrelativistic electron-positron annihilation is kinematically forbidden. In this case, the collision rates from the plasmon decay and the electron-positron scattering are expected to have similar patterns shown in Fig. 2.

The relation between the scattering and the forbidden decay can also have important consequences in the scenarios of right-handed neutrino DM production [3,66]. When the right-handed neutrino N_R is nonthermally produced by some forbidden decay at higher temperatures, the contribution from the related scattering sensitively depends on the mediator connecting the SM and N_R. If the mediator is the SM Higgs, which carries $\kappa \approx 0.4$ [57] from gauge and top Yukawa interactions, both the scattering and forbidden decay could contribute to the N_R production comparably [14]. However, if a right-handed neutrino only couples to a thermal scalar singlet that has a weaker connection to the SM plasma, it can be be inferred from Fig. 2 and Eq. (15) that the contribution from the forbidden decay would be much smaller than the scattering channel.

The out-of-equilibrium scattering production associated with the forbidden decay can also modify the thermally induced generation of lepton asymmetries in the early Universe [14,22–25]. If some forbidden decay is opened to produce N_R in a CP-violating way, the CP asymmetry stored in N_R can be transferred to the SM one, which in the active sphaleron epoch is partially converted into the baryon asymmetry. If the mediator carries a thermal parameter $\kappa \ll 1$, the scattering channel can be readily stronger than the forbidden decay.

V. CONCLUSION

We have illustrated a close relation between the forbidden decay and the associated scattering at finite temperatures. Instead of carrying higher- or lower-order weak coupling constants, the two-body scattering hinted from the forbidden decay diagram can carry the same order of coupling constants. For a light scalar mediator discussed in this paper, the close relation can be simply described by the dominant thermal coupling between the plasma and the mediator. Such a simple relation allows us to estimate the relative contribution to the DM relic density from the scattering and the forbidden decay. We found that the forbidden decay becomes important and can contribute to the total DM relic density at 5%–24% (10%–39%) for a thermal interaction in the weak-coupling regime and in the Boltzmann (quantum) statistics, but the scattering effect increases at the speed of inverse thermal coupling when the connection between the plasma and the mediator is much weaker.

Code and data availability. The code for obtaining the figures is publicly available at GitHub [67].

ACKNOWLEDGMENTS

The author thanks Oleg Lebedev, Katelin Schutz, and Xun-Jie Xu for valuable discussions. This work is supported in part by the National Natural Science Foundation of China under Grant No. 12141501.

[1] V. S. Rychkov and A. Strumia, Thermal production of gravitinos, Phys. Rev. D **75**, 075011 (2007).
[2] A. Strumia, Thermal production of axino dark matter, J. High Energy Phys. 06 (2010) 036.
[3] M. Drewes and J. U. Kang, Sterile neutrino dark matter production from scalar decay in a thermal bath, J. High Energy Phys. 05 (2016) 051.
[4] M. J. Baker, M. Breitbach, J. Kopp, and L. Mittnacht, Dynamic freeze-in: Impact of thermal masses and cosmological phase transitions on dark matter production, J. High Energy Phys. 03 (2018) 114.
[5] C. Dvorkin, T. Lin, and K. Schutz, Making dark matter out of light: Freeze-in from plasma effects, Phys. Rev. D **99**, 115009 (2019); **105**, 119901(E) (2022).
[6] L. Darmé, A. Hryczuk, D. Karamitros, and L. Roszkowski, Forbidden frozen-in dark matter, J. High Energy Phys. 11 (2019) 159.
[7] S. Biondini and J. Ghiglieri, Freeze-in produced dark matter in the ultra-relativistic regime, J. Cosmol. Astropart. Phys. 03 (2021) 075.
[8] P. Konar, R. Roshan, and S. Show, Freeze-in dark matter through forbidden channel in U(1)_B-L, J. Cosmol. Astropart. Phys. 03 (2022) 021.
[9] J. Bernstein, M. Ruderman, and G. Feinberg, Electromagnetic properties of the neutrino, Phys. Rev. **132**, 1227 (1963).
[10] E. Braaten and D. Segel, Neutrino energy loss from the plasma process at all temperatures and densities, Phys. Rev. D **48**, 1478 (1993).
[11] G. G. Raffelt, *Stars as Laboratories for Fundamental Physics: The Astrophysics of Neutrinos, Axions, and Other Weakly Interacting Particles* (University of Chicago Press, Chicago, 1996).
[12] D. G. Yakovlev, A. D. Kaminker, O. Y. Gnedin, and P. Haensel, Neutrino emission from neutron stars, Phys. Rep. **354**, 1 (2001).
[13] E. Hardy and R. Lasenby, Stellar cooling bounds on new light particles: Plasma mixing effects, J. High Energy Phys. 02 (2017) 033.
[14] G. F. Giudice, A. Notari, M. Raidal, A. Riotto, and A. Strumia, Towards a complete theory of thermal leptogenesis in the SM and MSSM, Nucl. Phys. **B685**, 89 (2004).
[15] M. Garny, A. Hohenegger, A. Kartavtsev, and M. Lindner, Systematic approach to leptogenesis in nonequilibrium QFT: Self-energy contribution to the *CP*-violating parameter, Phys. Rev. D **81**, 085027 (2010).
[16] M. Garny, A. Hohenegger, A. Kartavtsev, and M. Lindner, Systematic approach to leptogenesis in nonequilibrium QFT: Vertex contribution to the *CP*-violating parameter, Phys. Rev. D **80**, 125027 (2009).
[17] C. P. Kiessig, M. Plumacher, and M. H. Thoma, Decay of a Yukawa fermion at finite temperature and applications to leptogenesis, Phys. Rev. D **82**, 036007 (2010).
[18] M. Garny, A. Hohenegger, and A. Kartavtsev, Medium corrections to the *CP*-violating parameter in leptogenesis, Phys. Rev. D **81**, 085028 (2010).
[19] C. Kiessig and M. Plumacher, Hard-thermal-loop corrections in leptogenesis I: *CP*-asymmetries, J. Cosmol. Astropart. Phys. 07 (2012) 014.
[20] C. Kiessig and M. Plumacher, Hard-thermal-loop corrections in leptogenesis II: Solving the Boltzmann equations, J. Cosmol. Astropart. Phys. 09 (2012) 012.
[21] B. Garbrecht, Leptogenesis from additional Higgs doublets, Phys. Rev. D **85**, 123509 (2012).
[22] T. Hambye and D. Teresi, Higgs Doublet Decay as the Origin of the Baryon Asymmetry, Phys. Rev. Lett. **117**, 091801 (2016).
[23] T. Hambye and D. Teresi, Baryogenesis from L-violating Higgs-doublet decay in the density-matrix formalism, Phys. Rev. D **96**, 015031 (2017).
[24] S.-P. Li, X.-Q. Li, X.-S. Yan, and Y.-D. Yang, Freeze-in Dirac neutrinogenesis: Thermal leptonic *CP* asymmetry, Eur. Phys. J. C **80**, 1122 (2020).
[25] S.-P. Li, X.-Q. Li, X.-S. Yan, and Y.-D. Yang, Baryogenesis from hierarchical Dirac neutrinos, Phys. Rev. D **104**, 115014 (2021).
[26] M. Fukugita and S. Yazaki, Reexamination of astrophysical and cosmological constraints on the magnetic moment of neutrinos, Phys. Rev. D **36**, 3817 (1987).
[27] P. Elmfors, K. Enqvist, G. Raffelt, and G. Sigl, Neutrinos with magnetic moment: Depolarization rate in plasma, Nucl. Phys. **B503**, 3 (1997).
[28] A. Ayala, J. C. D'Olivo, and M. Torres, Right-handed neutrino production in dense and hot plasmas, Nucl. Phys. **B564**, 204 (2000).
[29] S.-P. Li and X.-J. Xu, Neutrino magnetic moments meet precision $N_{\rm eff}$ measurements, J. High Energy Phys. 02 (2023) 085.
[30] A. Boyarsky, V. Cheianov, O. Ruchayskiy, and O. Sobol, Evolution of the Primordial Axial Charge across Cosmic Times, Phys. Rev. Lett. **126**, 021801 (2021).
[31] A. Boyarsky, V. Cheianov, O. Ruchayskiy, and O. Sobol, Equilibration of the chiral asymmetry due to finite electron mass in electron-positron plasma, Phys. Rev. D **103**, 013003 (2021).
[32] J. McDonald, Thermally Generated Gauge Singlet Scalars as Selfinteracting Dark Matter, Phys. Rev. Lett. **88**, 091304 (2002).
[33] A. Kusenko, Sterile Neutrinos, Dark Matter, and the Pulsar Velocities in Models with a Higgs Singlet, Phys. Rev. Lett. **97**, 241301 (2006).
[34] K. Petraki and A. Kusenko, Dark-matter sterile neutrinos in models with a gauge singlet in the Higgs sector, Phys. Rev. D **77**, 065014 (2008).
[35] L. J. Hall, K. Jedamzik, J. March-Russell, and S. M. West, Freeze-In production of FIMP dark matter, J. High Energy Phys. 03 (2010) 080.
[36] N. Bernal, M. Heikinheimo, T. Tenkanen, K. Tuominen, and V. Vaskonen, The dawn of FIMP dark matter: A review of models and constraints, Int. J. Mod. Phys. A **32**, 1730023 (2017).
[37] J. H. Chang, R. Essig, and A. Reinert, Light(ly)-coupled dark matter in the keV range: Freeze-in and constraints, J. High Energy Phys. 03 (2021) 141.
[38] X. Chu, T. Hambye, and M. H. G. Tytgat, The four basic ways of creating dark matter through a portal, J. Cosmol. Astropart. Phys. 05 (2012) 034.

[39] S. Davidson, S. Hannestad, and G. Raffelt, Updated bounds on millicharged particles, J. High Energy Phys. 05 (2000) 003.
[40] J. H. Chang, R. Essig, and S. D. McDermott, Supernova 1987A constraints on Sub-GeV dark sectors, millicharged particles, the QCD axion, and an axion-like particle, J. High Energy Phys. 09 (2018) 051.
[41] M. Drewes *et al.*, A white paper on keV sterile neutrino dark matter, J. Cosmol. Astropart. Phys. 01 (2017) 025.
[42] A. Boyarsky, M. Drewes, T. Lasserre, S. Mertens, and O. Ruchayskiy, Sterile neutrino dark matter, Prog. Part. Nucl. Phys. **104**, 1 (2019).
[43] J. L. Feng, H. Tu, and H.-B. Yu, Thermal relics in hidden sectors, J. Cosmol. Astropart. Phys. 10 (2008) 043.
[44] A. Berlin, D. Hooper, and G. Krnjaic, Thermal dark matter from a highly decoupled sector, Phys. Rev. D **94**, 095019 (2016).
[45] A. D. Dolgov and F. L. Villante, BBN bounds on active sterile neutrino mixing, Nucl. Phys. **B679**, 261 (2004).
[46] S.-P. Li and X.-J. Xu, Dark matter produced from right-handed neutrinos, J. Cosmol. Astropart. Phys. 06 (2023) 047.
[47] M. Bellac, *Thermal Field Theory* (Cambridge University Press, Cambridge, England, 2000).
[48] P. Gondolo and G. Gelmini, Cosmic abundances of stable particles: Improved analysis, Nucl. Phys. **B360**, 145 (1991).
[49] P. B. Arnold, G. D. Moore, and L. G. Yaffe, Effective kinetic theory for high temperature gauge theories, J. High Energy Phys. 01 (2003) 030.
[50] S.-P. Li, Dark matter freeze-in via a light thermal fermion mediator, J. Cosmol. Astropart. Phys. 05 (2023) 008.
[51] E. Braaten and R. D. Pisarski, Soft amplitudes in hot gauge theories: A general analysis, Nucl. Phys. **B337**, 569 (1990).
[52] J. Frenkel and J. C. Taylor, High temperature limit of thermal QCD, Nucl. Phys. **B334**, 199 (1990).
[53] E. Braaten and R. D. Pisarski, Simple effective Lagrangian for hard thermal loops, Phys. Rev. D **45**, R1827 (1992).
[54] M. E. Carrington, D.-f. Hou, and M. H. Thoma, Equilibrium and nonequilibrium hard thermal loop resummation in the real time formalism, Eur. Phys. J. C **7**, 347 (1999).
[55] N. P. Landsman and C. G. van Weert, Real and imaginary time field theory at finite temperature and density, Phys. Rep. **145**, 141 (1987).
[56] J. Ghiglieri, A. Kurkela, M. Strickland, and A. Vuorinen, Perturbative thermal QCD: Formalism and applications, Phys. Rep. **880**, 1 (2020).
[57] J. M. Cline, K. Kainulainen, and K. A. Olive, Protecting the primordial baryon asymmetry from erasure by sphalerons, Phys. Rev. D **49**, 6394 (1994).
[58] A. Pilaftsis and T. E. J. Underwood, Resonant leptogenesis, Nucl. Phys. **B692**, 303 (2004).
[59] J. M. Cline, K. Kainulainen, and D. Tucker-Smith, Electroweak baryogenesis from a dark sector, Phys. Rev. D **95**, 115006 (2017).
[60] G. Bélanger, F. Boudjema, A. Goudelis, A. Pukhov, and B. Zaldivar, micrOMEGAs5.0: Freeze-in, Comput. Phys. Commun. **231**, 173 (2018).
[61] V. De Romeri, D. Karamitros, O. Lebedev, and T. Toma, Neutrino dark matter and the Higgs portal: Improved freeze-in analysis, J. High Energy Phys. 10 (2020) 137.
[62] K. Ala-Mattinen, M. Heikinheimo, K. Kainulainen, and K. Tuominen, Momentum distributions of cosmic relics: Improved analysis, Phys. Rev. D **105**, 123005 (2022).
[63] T. Bringmann, S. Heeba, F. Kahlhoefer, and K. Vangsnes, Freezing-in a hot bath: Resonances, medium effects and phase transitions, J. High Energy Phys. 02 (2022) 110.
[64] L. Husdal, On effective degrees of freedom in the early universe, Galaxies **4**, 78 (2016).
[65] N. Aghanim *et al.* (Planck Collaboration), Planck 2018 results. VI. Cosmological parameters, Astron. Astrophys. **641**, A6 (2020); **652**, C4(E) (2021).
[66] D. Besak and D. Bodeker, Thermal production of ultra-relativistic right-handed neutrinos: Complete leading-order results, J. Cosmol. Astropart. Phys. 03 (2012) 029.
[67] https://github.com/Shao-Ping-Li/Scattering_vs_Forbidden_Decay.